

Improved constraints on the mixing and mass of Z' bosons from resonant diboson searches at the LHC at $\sqrt{s} = 13$ TeV and predictions for Run II

I. D. Bobovnikov*

*Deutsches Elektronen-Synchrotron DESY, Notkestrasse 85, Hamburg 22607, Germany
and The Abdus Salam ICTP Affiliated Centre, Technical University of Gomel, 246746 Gomel, Belarus*

P. Osland†

Department of Physics and Technology, University of Bergen, Postboks 7803, N-5020 Bergen, Norway

A. A. Pankov‡

*The Abdus Salam ICTP Affiliated Centre, Technical University of Gomel, 246746 Gomel, Belarus
Institute for Nuclear Problems, Belarusian State University, 220030 Minsk, Belarus
and Joint Institute for Nuclear Research, Dubna 141980, Russia*

 (Received 30 September 2018; published 28 November 2018)

New neutral vector bosons Z' decaying to charged gauge boson pairs W^+W^- are predicted in many scenarios of new physics, including models with an extended gauge sector such as E_6 , left-right symmetric Z'_{LRS} and the sequential standard model Z'_{SSM} . For these benchmark models we calculate and present theoretical expectations for different values of the Z' mass M_2 and mixing parameter ξ . Our results are based on the narrow width approximation which allows for the making of a convenient comparison of the experiment to theoretical benchmark models. The diboson production allows for the placement of stringent constraints on the Z - Z' mixing angle and the Z' mass, which we determine by using data from pp collisions at $\sqrt{s} = 13$ TeV recorded by the ATLAS detector at the CERN LHC, with integrated luminosity of $\sim 36 \text{ fb}^{-1}$. By comparing the experimental limits to the theoretical predictions for the total cross section of Z' resonant production and its subsequent decay into W^+W^- pairs, we show that the derived constraints on the mixing angle for the benchmark models are of the order of a few $\times 10^{-4}$, i.e., greatly improved with respect to those derived from the global analysis of electroweak data. We combine the limits derived from diboson production data with those obtained from the Drell–Yan process in order to significantly extend the exclusion region in the M_2 - ξ parameter plane. Also, we demonstrate that further improvement on the constraining of this mixing can be achieved through analysis of the full set of Run II data.

DOI: [10.1103/PhysRevD.98.095029](https://doi.org/10.1103/PhysRevD.98.095029)

I. INTRODUCTION

Neutral vector bosons, Z' , are among the best motivated scenarios of physics beyond the Standard Model (SM) [1]. Many new physics models beyond the SM [2], including superstring and left-right-symmetric models, predict the existence of such bosons. They might actually be light enough to be accessible at current and/or future colliders. The search for such neutral Z' gauge bosons is an important

aspect of the experimental physics program of present and future high-energy colliders.

Limits from direct production at the LHC and virtual effects at the Large Electron-Positron Collider (LEP), through interference or mixing with the Z boson, imply that any new Z' boson is rather heavy and mixes very little with the Z boson. Depending on the considered theoretical model, Z' masses of the order of 4.5 TeV [3,4] and Z - Z' mixing angles at the level of 10^{-3} are already excluded [5,6] (see also [7,8]). These constraints come from the very high-precision Z pole experiments at LEP and the Stanford Linear Collider (SLC) [9], including measurements from the Z line shape, from the leptonic branching ratios (normalized to the total hadronic Z decay width) as well as from leptonic forward-backward asymmetries. While these experiments were virtually blind to Z' bosons with negligible Z - Z' mixing, precision measurements at lower and higher energies (away from the Z pole) attainable at

*boboilya@yandex.by

†Per.Osland@uib.no

‡pankov@ictp.it

Published by the American Physical Society under the terms of the Creative Commons Attribution 4.0 International license. Further distribution of this work must maintain attribution to the author(s) and the published article's title, journal citation, and DOI. Funded by SCOAP³.

TRISTAN [10] and LEP2 [11], respectively, were able to probe the Z' exchange amplitude via its interference with the photon and the SM Z boson.

However, as was shown in [12], the LHC at nominal collider energy of $\sqrt{s} = 14$ TeV and integrated luminosity of $\mathcal{L}_{\text{int}} = 100 \text{ fb}^{-1}$ has a high potential to improve significantly on the current limits on the Z - Z' mixing angle in the diboson channel:

$$pp \rightarrow (Z_2 \rightarrow W^+W^-) + X. \quad (1)$$

This was demonstrated in a recent paper [13] for the ‘‘Altarelli Reference Model’’ [14], also known as the Sequential Standard Model (SSM), by using the current ATLAS [15] and CMS [16] data collected at a center-of-mass energy of $\sqrt{s} = 13$ TeV during searches for resonant W^+W^- diboson production. The SSM is often taken as a convenient benchmark by experimentalists [17]. In this model, the new heavy gauge bosons Z'_{SSM} are considered heavy carbon copies of the familiar Z , with the same coupling constants.

In ATLAS W^+W^- events are reconstructed via their semileptonic decays, where one W boson decays into a charged lepton ($l = e, \mu$) and a neutrino, and the other into two jets [15]. CMS collects data where both W bosons decay hadronically with two reconstructed jets (dijet channel) [16]. The analysis presented below is based on pp collision data at a center-of-mass energy $\sqrt{s} = 13$ TeV, collected by the ATLAS experiment (36.1 fb^{-1}). We consider here information provided by ATLAS in published papers and in the HEPDATA database [18]. We shall also comment on the corresponding CMS result [16]. The data is used to probe the Z - Z' mixing and to interpret the results of the present analysis within models with an extended gauge sector. Among these, models based on the E_6 GUT group and left-right symmetry groups have been extensively pursued in the literature and are particularly significant from the point of view of LHC phenomenology. Here we extend our analysis presented in [13] for the SSM to various Z' models, which include the E_6 based $Z'_\chi, Z'_\psi, Z'_\eta$, and also the Z'_{LRS} boson appearing in models with left-right symmetry. Thus, our present analysis is complementary to the previous studies [13].

One should emphasize that we made a choice of particular benchmark models to represent different qualitative features of those Z' models, such as the fact that those models typically involve an extra neutral Z' boson with relatively narrow width (which however may become larger if non-SM particles are included in the decays in addition to the SM states).

The W^+W^- pair production process (1) is very important for diagnostics of the electroweak gauge symmetry. General properties of the weak gauge bosons are closely related to electroweak symmetry breaking and to the

structure of the gauge sector, like the existence and structure of trilinear couplings. Also, the diboson decay mode of the Z' probes the gauge coupling strength between the new and the SM gauge bosons [12,13,19–21]. In addition, the coupling strength strongly influences the decay branching ratios and the natural widths of such a new gauge boson. Thus, detailed examination of the process (1) will not only test the gauge sector of the SM with high accuracy, it will also shed light on any new physics (NP) that may appear beyond the SM. Here, we examine the feasibility of observing Z' boson effects in the W^+W^- pair production process at the LHC.

In contrast to the Drell-Yan (DY) process

$$pp \rightarrow Z' \rightarrow \ell^+\ell^- + X, \quad (2)$$

with $\ell = e, \mu$, the diboson process is not the principal discovery channel, but can help to understand the origin of new gauge bosons.

At Tevatron energies, direct searches for heavy W^+W^- resonances have been performed by both the CDF and D0 collaborations. The D0 collaboration explored diboson resonant production up to masses $\sim \mathcal{O}(700 \text{ GeV})$ using the pure leptonic $\ell\nu\ell'\nu'$ and semileptonic $\ell\nu jj$ final states [22]. On the other hand, the CDF collaboration searched for resonant W^+W^- production in the $\ell\nu jj$ final state, resulting in a lower limit on the masses of Z' and W' bosons [7], excluding masses up to $\mathcal{O}(900 \text{ GeV})$, depending on the mixing.

Previous searches for diboson (VV) resonances at the LHC were carried out by the ATLAS and CMS collaborations with pp collisions at $\sqrt{s} = 7, 8$ and 13 TeV. These include fully leptonic ($\ell\nu\ell\nu, \ell\nu\ell\ell$) [23–26], semileptonic ($\nu\nu jj, \ell\nu jj, \ell\ell jj$) [27–29] and fully hadronic ($jjjj$) VV [27,29] final states. By combining the results of searches in the $\nu\nu jj, \ell\nu jj, \ell\ell jj$ and $jjjj$ channels, the ATLAS collaboration [27] set a lower bound of 2.60 TeV on the mass of a spin-1 resonance at the 95% confidence level, in the context of the heavy vector triplet model. The recent results presented in [15,16] by the ATLAS and CMS collaborations using, respectively, semileptonic and hadronic final-state events in pp collision data at 13 TeV benefit from an integrated luminosity of $\sim 36 \text{ fb}^{-1}$, which is an order of magnitude larger than what was available for the previous search in the fully hadronic final state at $\sqrt{s} = 13$ TeV [27].

It should be noted that the future e^+e^- International Linear Collider (ILC) with high c.m. energies and longitudinally polarized beams could indicate the existence of Z' bosons via its interference effects in fermion pair production processes, with masses up to about $6 \times \sqrt{s}$ [30] while Z - Z' mixing will be constrained down to $\sim 10^{-4}$ – 10^{-3} in the process $e^+e^- \rightarrow W^+W^-$ [20].

In this work, we derive bounds on a possible new neutral spin-1 resonance (Z') for the considered models from the available ATLAS data on W^+W^- pair production [15]. We present results as constraints on the relevant Z - Z' mixing angle introduced in Sec. II and on the $M_{Z'}$ mass.

The paper is organized as follows. In Sec. II, we briefly describe the Z - Z' mixing and emphasize its role in the process (1). In Sec. III we summarize the relevant cross section, in Sec. IV we study the $Z_2 \rightarrow W^+W^-$ width, and then in Sec. V we show the resulting constraints on the M_2 - ξ parameter space, whereas in Sec. VI we discuss results from the DY process $q\bar{q} \rightarrow Z_2 \rightarrow l^+l^-$. In Sec. VII we collect and compare constraints from the diboson process with those deduced from the Drell–Yan process, and in Sec. VIII we conclude.

II. Z-Z' MIXING

Signals of Z' in representative models such as the E_6 models, the Left-Right (LR) model and the SSM have been extensively studied in the literature [1] and explored at LEP2, the Tevatron and the LHC. For the present notation we refer to [20], where also a brief description of the models can be found.

The mass-squared matrix of the Z and Z' can have nondiagonal entries δM^2 , which are related to the vacuum expectation values of the fields of an extended Higgs sector:

$$M_{ZZ'}^2 = \begin{pmatrix} M_Z^2 & \delta M^2 \\ \delta M^2 & M_{Z'}^2 \end{pmatrix}. \quad (3)$$

Here, Z and Z' denote the weak gauge boson eigenstates of $SU(2)_L \times U(1)_Y$ and of the extra $U(1)'$, respectively. The mass eigenstates, Z_1 and Z_2 , which diagonalize the matrix (3), are obtained by a rotation of the fields Z and Z' :

$$Z_1 = Z \cos \phi + Z' \sin \phi, \quad (4a)$$

$$Z_2 = -Z \sin \phi + Z' \cos \phi. \quad (4b)$$

The mixing angle ϕ is expressed in terms of masses as [1]:

$$\tan^2 \phi = \frac{M_Z^2 - M_1^2}{M_2^2 - M_Z^2} \simeq \frac{2M_Z \Delta M}{M_2^2}, \quad (5)$$

where the downward shift $\Delta M = M_Z - M_1 > 0$, M_Z being the mass of the Z_1 boson in the absence of mixing, i.e., for $\phi = 0$. We assume the mass M_1 is determined experimentally; the mixing then depends on two free parameters, which we identify as ϕ and M_2 , and we will adopt this parametrization throughout the paper. In the important limit $M_{Z'} \gg (M_Z, \Delta M)$ one finds [1]

$$M_1 \sim M_Z \ll M_{Z'} \sim M_2. \quad (6)$$

The mixing angle ϕ will play an important role in our analysis. Such mixing effects reflect the underlying gauge symmetry and/or the Higgs sector of the model. For instance, in certain models one specifies not only the $SU(2)$ assignments but the $U(1)'$ assignments of the Higgs fields. To a good approximation, for $M_1 \ll M_2$, in specific ‘‘minimal Higgs’’ models, one has an additional constraint [31]:

$$\phi \simeq -s_W^2 \frac{\sum_i \langle \Phi_i \rangle^2 I_{3L}^i Q_i'}{\sum_i \langle \Phi_i \rangle^2 (I_{3L}^i)^2} = C \frac{M_1^2}{M_2^2}, \quad (7)$$

where s_W is the sine of the electroweak angle. In these models ϕ and M_2 are not independent and there is only one (e.g., M_2) free parameter. Furthermore, $\langle \Phi_i \rangle$ are the Higgs vacuum expectation values spontaneously breaking the symmetry, and Q_i' are their charges with respect to the additional $U(1)'$. In these models the same Higgs multiplets are responsible for both generation of the mass M_1 and for the strength of the Z - Z' mixing. Thus C is a model-dependent constant.

From (4), one obtains the vector and axial-vector couplings of the Z_1 and Z_2 bosons to fermions:

$$v_{1f} = v_f \cos \phi + v'_f \sin \phi, \quad a_{1f} = a_f \cos \phi + a'_f \sin \phi, \quad (8a)$$

$$v_{2f} = v'_f \cos \phi - v_f \sin \phi, \quad a_{2f} = a'_f \cos \phi - a_f \sin \phi, \quad (8b)$$

with v'_f and a'_f the fermionic Z' couplings which can be found, e.g., in [20].

We will consider NP models where Z' 's interact with charged gauge bosons W^\pm via their mixing with the SM Z , assuming that the Z' couplings exhibit the same Lorentz structure as those of the SM. An important property of the models under consideration is that the gauge eigenstate Z' does not couple to the W^+W^- pair since it is neutral under $SU(2)_L$. Therefore the process (1) is sensitive to a Z' only in the case of a nonzero Z - Z' mixing. From (4a) and (4b), one obtains:

$$g_{WWZ_1} = \cos \phi g_{WWZ}, \quad (9a)$$

$$g_{WWZ_2} = -\sin \phi g_{WWZ}, \quad (9b)$$

where $g_{WWZ} = \cot \theta_W$.¹ Also, $g_{WW\gamma} = 1$.

¹In our analysis, we ignore kinetic mixing [32]. Such mixing would introduce an additional parameter and could modify the exclusion reach (see, e.g., [33,34]).

In many extended gauge models, while the couplings to fermions are not much different from those of the SM, the $Z_2 WW$ coupling is substantially suppressed with respect to that of the SM. In fact, in the extended gauge models the SM trilinear gauge boson coupling strength, g_{WWZ} , is replaced by $g_{WWZ} \rightarrow \xi \cdot g_{WWZ}$, where $\xi \equiv |\sin \phi|$ [see Eq. (9b)] is the mixing factor. We will set cross section limits on such Z_2 as functions of the mass M_2 and ξ .

III. CROSS SECTION

The differential cross section for the process (1) from initial quark-antiquark states can be written as

$$\frac{d\sigma}{dM dy dz} = K \frac{2M}{s} \sum_q [f_{q|P_1}(\xi_1) f_{\bar{q}|P_2}(\xi_2) + f_{\bar{q}|P_1}(\xi_1) f_{q|P_2}(\xi_2)] \frac{d\hat{\sigma}_{q\bar{q}}}{dz}. \quad (10)$$

Here, s denotes the proton-proton center-of-mass energy squared, $z \equiv \cos \theta$, with θ the W^- -boson-quark angle in the W^+W^- center-of-mass frame, y the diboson rapidity and M the diboson W^+W^- invariant mass. Furthermore, $f_{q|P_1}(\xi_1, M)$ and $f_{\bar{q}|P_2}(\xi_2, M)$ are quark and antiquark distribution functions for the protons P_1 and P_2 , respectively, with $\xi_{1,2} = (M/\sqrt{s}) \exp(\pm y)$ the parton fractional momenta. Finally, $d\hat{\sigma}_{q\bar{q}}/dz$ are the partonic differential cross sections, to be specified below. In (10), the K factor accounts for higher-order QCD contributions. For numerical computation, we use the CTEQ-6L1 parton distributions [35]. Our estimates will be at the Born level, thus the factorization scale μ_F enters only through the parton distribution functions, as the parton-level cross section at this order does not depend on μ_F . As regards the scale dependence of the parton distributions we choose for

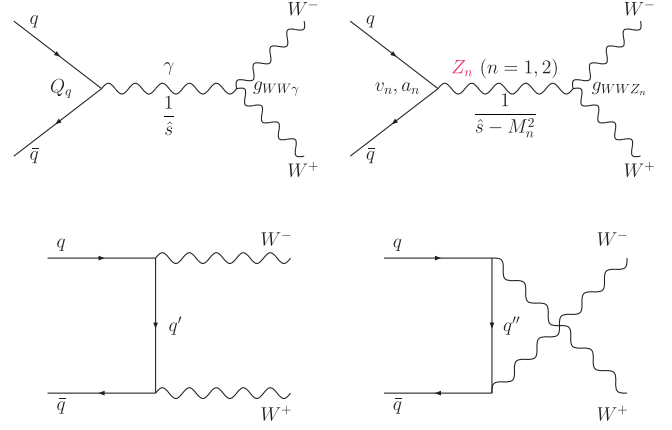


FIG. 1. Leading-order Feynman diagrams for the $q\bar{q} \rightarrow \gamma, Z_1, Z_2 \rightarrow W^+W^-$ process within the framework of extended gauge models.

the factorization scale the W^+W^- invariant mass, $\mu_F^2 = M^2 = \hat{s}$, with $\hat{s} = \xi_1 \xi_2 s$ the parton subprocess c.m. energy squared. The obtained constraints presented in the following are numerically, not significantly modified when μ_F is varied in the range from $\mu_F/2$ to $2\mu_F$.

The parton-level W^+W^- boson pair production can be described, within the gauge models discussed here, by the subprocesses [12]

$$q\bar{q} \rightarrow \gamma, Z_1, Z_2 \rightarrow W^+W^-, \quad (11)$$

as well as t - and u -channel Feynman diagrams displayed in Fig. 1.

The differential cross section for the processes $q\bar{q} \rightarrow W^+W^-$ described by Feynman diagrams depicted in Fig. 1 and averaged over quark colors can be written as [2]

$$\begin{aligned} \left(\frac{\pi\alpha_{\text{em}}^2\beta_W}{N_C\hat{s}}\right)^{-1} \frac{d\hat{\sigma}_{q\bar{q}}}{dz} &= [(Q_q + v_{1q}g_{WWZ_1}\chi_1 + v_{2q}g_{WWZ_2}\chi_2)^2 + (a_{1q}g_{WWZ_1}\chi_1 + a_{2q}g_{WWZ_2}\chi_2)^2]A(\hat{s}, \hat{t}, \hat{u}) \\ &+ \frac{1}{2\hat{s}_W^2} [Q_q + (v_{1q} + a_{1q})g_{WWZ_1}\chi_1 + (v_{2q} + a_{2q})g_{WWZ_2}\chi_2] [\theta(-Q_q)I(\hat{s}, \hat{t}, \hat{u}) - \theta(Q_q)I(\hat{s}, \hat{u}, \hat{t})] \\ &+ \frac{1}{8\hat{s}_W^4} [\theta(-Q_q)E(\hat{s}, \hat{t}, \hat{u}) + \theta(Q_q)E(\hat{s}, \hat{u}, \hat{t})], \end{aligned} \quad (12)$$

where $\alpha_{\text{em}} = 1/128.9$, $\theta(x) = 1$ for $x > 0$ and $\theta(x) = 0$ for $x < 0$, N_C being the color factor ($N_C = 3$ for quarks), and

$$\begin{aligned} A(\hat{s}, \hat{t}, \hat{u}) &= \left(\frac{\hat{t}\hat{u}}{M_W^4} - 1\right) \left(\frac{1}{4} - \frac{M_W^2}{\hat{s}} + 3\frac{M_W^4}{\hat{s}^2}\right) + \frac{\hat{s}}{M_W^2} - 4, \\ I(\hat{s}, \hat{t}, \hat{u}) &= \left(\frac{\hat{t}\hat{u}}{M_W^4} - 1\right) \left(\frac{1}{4} - \frac{M_W^2}{2\hat{s}} - \frac{M_W^4}{\hat{s}\hat{t}}\right) + \frac{\hat{s}}{M_W^2} - 2 + 2\frac{M_W^2}{\hat{t}}, \\ E(\hat{s}, \hat{t}, \hat{u}) &= \left(\frac{\hat{t}\hat{u}}{M_W^4} - 1\right) \left(\frac{1}{4} + \frac{M_W^4}{\hat{t}^2}\right) + \frac{\hat{s}}{M_W^2}. \end{aligned} \quad (13)$$

Here, \hat{s} , \hat{t} , \hat{u} are the Mandelstam variables defined as $\hat{s} = M^2$, $\hat{t} = M_W^2 - \hat{s}(1 - \beta_W z)/2$, $\hat{u} = M_W^2 - \hat{s}(1 + \beta_W z)/2$; $\chi_1 = \hat{s}/(\hat{s} - M_1^2 + iM_1\Gamma_1)$, $\chi_2 = \hat{s}/(\hat{s} - M_2^2 + iM_2\Gamma_2)$, $\Gamma_{1,2}$ are total $Z_{1,2}$ boson decay widths; and $\gamma_W = \sqrt{\hat{s}}/2M_W$. In the t - and u -channel exchanges of Fig. 1 we account for the initial $q = u, d, s, c$, only the Cabibbo-Kobayashi-Maskawa favored quarks in the approximation of unity relevant matrix element. The differential cross section for the processes $q\bar{q} \rightarrow W^+W^-$ in the SM [2] can be reproduced from Eq. (12) if one ignores the effects of the Z - Z' mixing.

The differential cross section for the process $q\bar{q} \rightarrow Z_2 \rightarrow W^+W^-$, averaged over quark colors, can now be obtained from Eq. (12) and written as [12]

$$\frac{d\hat{\sigma}_{q\bar{q}}^{Z_2}}{d\cos\theta} = \frac{1}{3} \frac{\pi\alpha_{\text{em}}^2 \cot^2\theta_W}{16\hat{s}} \beta_W^3 (v_{2,f}^2 + a_{2,f}^2) |\chi_2|^2 \times \left(\frac{\hat{s}^2}{M_W^4} \sin^2\theta + 4 \frac{\hat{s}}{M_W^2} (4 - \sin^2\theta) + 12 \sin^2\theta \right) \cdot \xi^2. \quad (14)$$

The resonant production cross section of process (1) at the hadronic level can be derived from Eqs. (10) and (14). Specifically, the total cross section for the narrow Z_2 state is derived from (10) by integrating the right-hand side over the full phase space. In the narrow width approximation (NWA), one obtains [12]:

$$\sigma^{Z_2} = \sigma(pp \rightarrow Z_2) \times \text{Br}(Z_2 \rightarrow W^+W^-), \quad (15)$$

where $\sigma(pp \rightarrow Z_2) \times \text{Br}(Z_2 \rightarrow W^+W^-)$ is the (theoretical) total Z_2 production cross section times branching ratio determined in the total phase space.

However, it turns out that the real situation is more complicated because the cross section for W^+W^- pair production is measured indirectly via decay products of W 's. In fact, the analysis performed in Sec. V is based on the available ATLAS data of W^+W^- pair production with their subsequent decay into semileptonic final states [15] where one W boson decays leptonically ($W \rightarrow \ell\nu$ with $\ell = e, \mu$) and the other W boson decays hadronically ($W \rightarrow q\bar{q}'$ with q, q' quarks) which can be written as $pp \rightarrow Z_2 \rightarrow W^+W^- \rightarrow \ell^\pm jj\cancel{E}_T$, where j stands for jets.

The cross section is measured in a fiducial phase space and also in the total phase space (see, e.g., [23,36]). The fiducial cross section $\sigma_{\text{fid}}^{Z_2}$ for the $pp \rightarrow Z_2 \rightarrow W^+W^- \rightarrow \ell^\pm jj\cancel{E}_T$ process is calculated according to the equation

$$\sigma_{\text{fid}}^{Z_2} = \frac{N_{\text{data}} - N_{\text{bkg}}}{\varepsilon \times \mathcal{L}_{\text{int}}} = \frac{N^{Z_2}}{\varepsilon \times \mathcal{L}_{\text{int}}}, \quad (16)$$

where N_{data} and N_{bkg} are the number of observed data events and estimated background events, respectively, N^{Z_2}

is the number of signal events for a narrow Z_2 resonance state, ε is defined as the ratio of the number of events satisfying all selection criteria to the number of events produced in the fiducial phase space and is estimated from simulation. \mathcal{L}_{int} is the integrated luminosity of the data sample.

The total cross section σ^{Z_2} for the $pp \rightarrow Z_2 \rightarrow W^+W^- + X$ process is calculated for each channel using the equation

$$\sigma^{Z_2} = \frac{N^{Z_2}}{\varepsilon \times A \times \text{BR} \times \mathcal{L}_{\text{int}}}, \quad (17)$$

where A represents the kinematic and geometric acceptance from the total phase space to the fiducial phase space, and BR is the branching ratio for both W bosons decaying into $l\nu \oplus jj$. In other words, the overall acceptance, times trigger, reconstruction and selection efficiencies ($A \times \varepsilon$) are defined as the number of signal events passing the full event selection divided by the number of generated events. The total cross section σ^{Z_2} is this physical quantity that is measured experimentally at the LHC and which will be used in our analysis performed in Sec. V.

IV. THE Z_2 WIDTH

In the calculation of the total width Γ_2 we consider the following channels: $Z_2 \rightarrow f\bar{f}$, W^+W^- , and Z_1H [37], where H is the SM Higgs boson and f are the SM fermions ($f = l, \nu, q$). Throughout the paper we shall ignore the couplings of the Z_2 to beyond-SM particles such as right-handed neutrinos, SUSY partners and any exotic fermions in the theory, which all together may increase the width of the Z_2 by up to about a factor of five [38] and hence lower the branching ratio into a W^+W^- pair by the same factor.

The total width Γ_2 of the Z_2 boson can be written as follows:

$$\Gamma_2 = \sum_f \Gamma_2^{ff} + \Gamma_2^{WW} + \Gamma_2^{Z_1H}. \quad (18)$$

The presence of the two last decay channels, which are often neglected at low and moderate values of M_2 , is due to Z - Z' mixing. Note that the widths of these two bosonic modes W^+W^- and Z_1H do not depend on unknown masses of the final states such as heavy scalars that may enter in some other exotic diboson channels which we here ignore.

TABLE I. Ratio Γ_2^{ff}/M_2 for the χ, ψ, η , LRS and SSM models.

Z_2	Γ_2/M_2 [%]
χ	1.2
ψ	0.5
η	0.6
LRS	2.0
SSM	3.0

TABLE II. Constraints on the Z - Z' mixing parameter ξ at 95% C.L. in different models, processes and experiments.

Collider, process	Model	Z'_χ	Z'_ψ	Z'_η	Z'_{LRS}	Z'_{SSM}	@ M_2 (TeV)
LEP2, $e^+e^- \rightarrow W^+W^-$ [8]	$\xi[10^{-2}]$	6	15	50	12	7	≥ 1
Tevatron, $p\bar{p} \rightarrow W^+W^- + X$ [7]	$\xi[10^{-2}]$	2	0.4–0.9
electroweak (EW) data [5]	$\xi^{\text{EW}}[10^{-3}]$	1.6	1.8	4.7	1.3	2.6	...
LHC@13 TeV, W^+W^- ATLAS data with 36.1 fb $^{-1}$ (this work)	$\xi[10^{-3}]$	0.6	0.5	0.4	0.5	0.4	0.5–5.0
LHC@13 TeV, W^+W^- Run II, (extrap. 150 fb $^{-1}$) (this work)	$\xi[10^{-3}]$	0.4	0.3	0.3	0.3	0.3	0.5–5.0
ILC@0.5 TeV, 0.5 ab $^{-1}$, $e^+e^- \rightarrow W^+W^-$ [20]	$\xi[10^{-3}]$	1.5	2.3	1.6	1.4	1.2	≥ 3
ILC@1.0 TeV, 1.0 ab $^{-1}$, $e^+e^- \rightarrow W^+W^-$ [20]	$\xi[10^{-3}]$	0.4	0.6	0.5	0.4	0.3	≥ 3

The fermion contribution, $\sum_f \Gamma_2^{ff}$, depends on the number n_g of generations of heavy exotic fermions which can contribute to the Z_2 decay without phase space suppression. This number is model dependent, too, and introduces a phenomenological uncertainty. For the range of M_2 values below ~ 3 – 4 TeV, the dependence of Γ_2 on the values of ξ (within its allowed range) induced by $\sum_f \Gamma_2^{ff}$, Γ_2^{WW} and $\Gamma_2^{Z_1H}$ is unimportant. Therefore, in this mass range, one can approximate the total width as $\Gamma_2 \approx \sum_f \Gamma_2^{ff}$, where the sum runs over SM fermions only. The ratios of Γ_2^{ff}/M_2 for the benchmark models are summarized in Table I. One can appreciate the narrowness of the Z_2 pole from this Table I.

However, for large Z_2 masses, $M_2 > 4$ TeV, there is an enhancement that cancels the suppression due to the tiny Z - Z' mixing parameter ξ [39]. While the ‘‘Equivalence theorem’’ [40] might suggest a value for $\text{Br}(Z_2 \rightarrow Z_1H)$ comparable to $\text{Br}(Z_2 \rightarrow W^+W^-)$ up to electroweak symmetry breaking effects and phase-space factors, the Z_2Z_1H coupling is quite model dependent [37,41]. We take an approach as model-independent as possible, and for numerical illustration show our results in two simple scenarios. In the first scenario (adopted in the bulk of the paper), we treat the model as effectively having a suppressed partial width of $Z_2 \rightarrow Z_1H$ with respect to that of $Z_2 \rightarrow W^+W^-$, i.e. $\Gamma_2^{Z_1H} \ll \Gamma_2^{WW}$, so that one can ignore the former. In this case, numerical results with our treatment will serve as an upper bound on the size of the signal. The second scenario concerns the situation when both partial widths are comparable, $\Gamma_2^{Z_1H} \simeq \Gamma_2^{WW}$ for heavy M_2 [37,41,42]. We will start our analysis from the first scenario and then make comments on the second one emphasizing the implication of the decay channel $Z_2 \rightarrow Z_1H$ for diboson resonance searches in the process (1) at the LHC. In that latter case, one can expect that Γ_2 would be larger, with a suppression in the branching ratio to W^+W^- , and the bounds from LHC (and the ability for observing the Z - Z' mixing effect) would be reduced.

Notice that for all M_2 values of interest for LHC the width of the Z_2 boson is considerably smaller than the experimental mass resolution ΔM for which we adopt the parametrization in reconstructing the diboson invariant mass of the W^+W^- system, $\Delta M/M \approx 5\%$, as proposed, e.g., in [27,43].

The expression for the partial width of the $Z_2 \rightarrow W^+W^-$ decay channel can be written as [14]:

$$\Gamma_2^{WW} = \frac{\alpha_{\text{em}}}{48} \cot^2 \theta_W M_2 \left(\frac{M_2}{M_W} \right)^4 \left(1 - 4 \frac{M_W^2}{M_2^2} \right)^{3/2} \times \left[1 + 20 \left(\frac{M_W}{M_2} \right)^2 + 12 \left(\frac{M_W}{M_2} \right)^4 \right] \cdot \xi^2. \quad (19)$$

The dominant term in the second line of Eq. (14), for $M^2 \gg M_W^2$, is proportional to $(M/M_W)^4 \sin^2 \theta$ and corresponds to the production of longitudinally polarized W 's, $Z_2 \rightarrow W_L^+ W_L^-$. This strong dependence on the invariant mass results in a very steep growth of the cross section with energy and therefore a substantial increase of the cross section sensitivity to Z - Z' mixing at high M . In its turn, for a fixed mixing factor ξ and at large M_2 where Γ_2^{WW} dominates over $\sum_f \Gamma_2^{ff}$ the total width increases rapidly² with the mass M_2 because of the quintic dependence on the Z_2 mass of the W^+W^- mode as shown in Eq. (19). In this case, the W^+W^- mode becomes dominant and $\text{Br}(Z_2 \rightarrow W^+W^-) \rightarrow 1$, while the fermionic decay channels ($\Gamma_2^{ff} \propto M_2$) are increasingly suppressed.

As was mentioned in Sec. I, for models based on the E_6 GUT and left-right symmetry groups, the Z - Z' mixing angles (and ξ) were excluded at the level of a few per mil [5]. These limits on the mixing parameter were obtained from an analysis of the Z' extended models under consideration against available electroweak (EW) precision data and are summarized in Table II.

All these features are demonstrated in Figs. 2–4, where we plot $\text{Br}(Z_2 \rightarrow W^+W^-)$ vs M_2 for various Z' models and mixing factor ξ ranging from 0.0005 to 0.01. As reference, we also show the branching ratio corresponding to $\xi = \xi^{\text{EW}}$, the bound obtained from the electroweak precision data [5]. Values of ξ larger than ξ^{EW} are shown only for illustrative purposes. It should be stressed that the boost of the branching ratio for high values of M_2 , illustrated in these figures, plays an important role in the following analysis.

²Here we follow the first scenario, assuming $\Gamma_2^{Z_1H} = 0$.

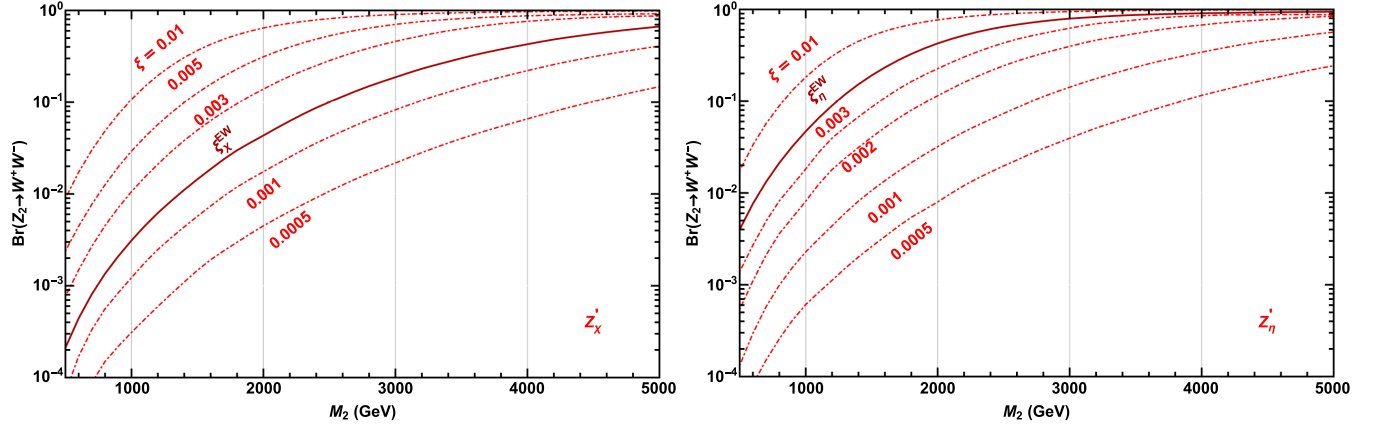


FIG. 2. Branching fraction $\text{Br}(Z_2 \rightarrow W^+W^-)$ vs M_2 for the χ model (left panel) and the η model (right panel). Labels attached to the curves correspond to a range of values of the mixing factor ξ from 0.01 and down to 0.0005, where values larger than the limits obtained from the electroweak precision data, $\xi_\chi^{\text{EW}} = 1.6 \times 10^{-3}$ in the left panel and $\xi_\eta^{\text{EW}} = 4.7 \times 10^{-3}$ in the right panel, are shown only for illustrative purposes.

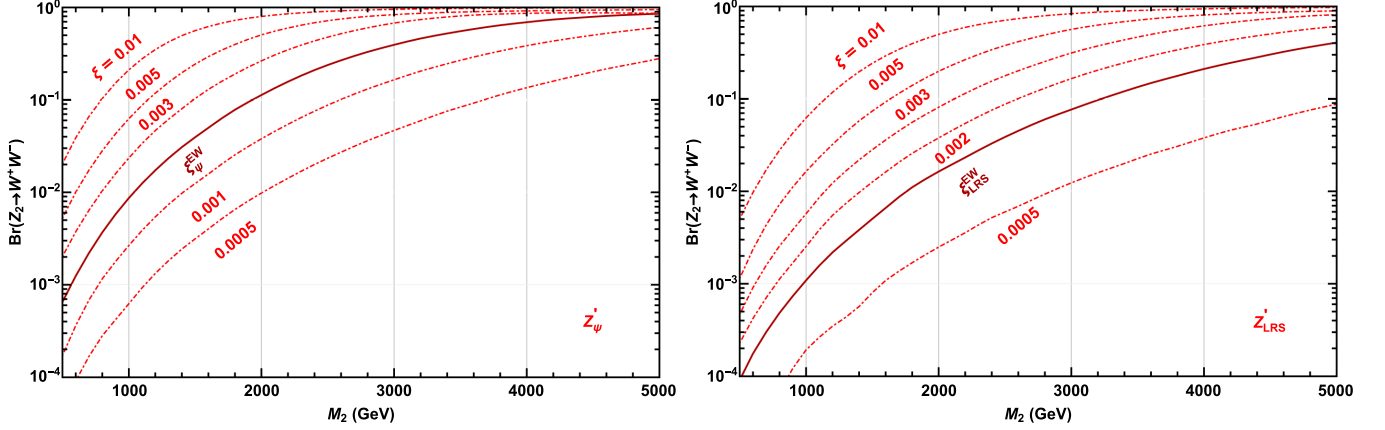


FIG. 3. Same as in Fig. 2 but for the ψ model with $\xi_\psi^{\text{EW}} = 1.8 \times 10^{-3}$ (left panel) and for the LRS model with $\xi_{\text{LRS}}^{\text{EW}} = 1.3 \times 10^{-3}$ (right panel).

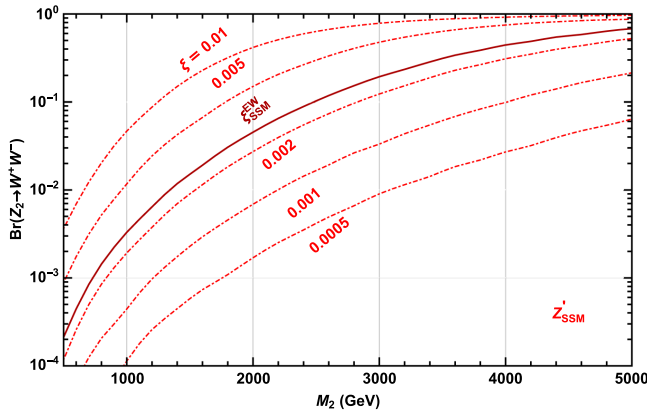


FIG. 4. Same as in Fig. 2 but for the SSM model with $\xi_{\text{SSM}}^{\text{EW}} = 2.6 \times 10^{-3}$.

We also note that the branching ratios of the different models are ordered in the following manner:

$$\begin{aligned} \text{Br}(Z_2 \rightarrow W^+W^-)_{\text{SSM}} &< \text{Br}(Z_2 \rightarrow W^+W^-)_{\text{LRS}} \\ &< \text{Br}(Z_2 \rightarrow W^+W^-)_\chi < \text{Br}(Z_2 \rightarrow W^+W^-)_\eta \\ &< \text{Br}(Z_2 \rightarrow W^+W^-)_\psi. \end{aligned} \quad (20)$$

This will be reflected in the bounds obtained.

V. CONSTRAINTS FROM THE DIBOSON PROCESS

Here, we present an analysis, employing the most recent measurements of diboson processes provided by ATLAS

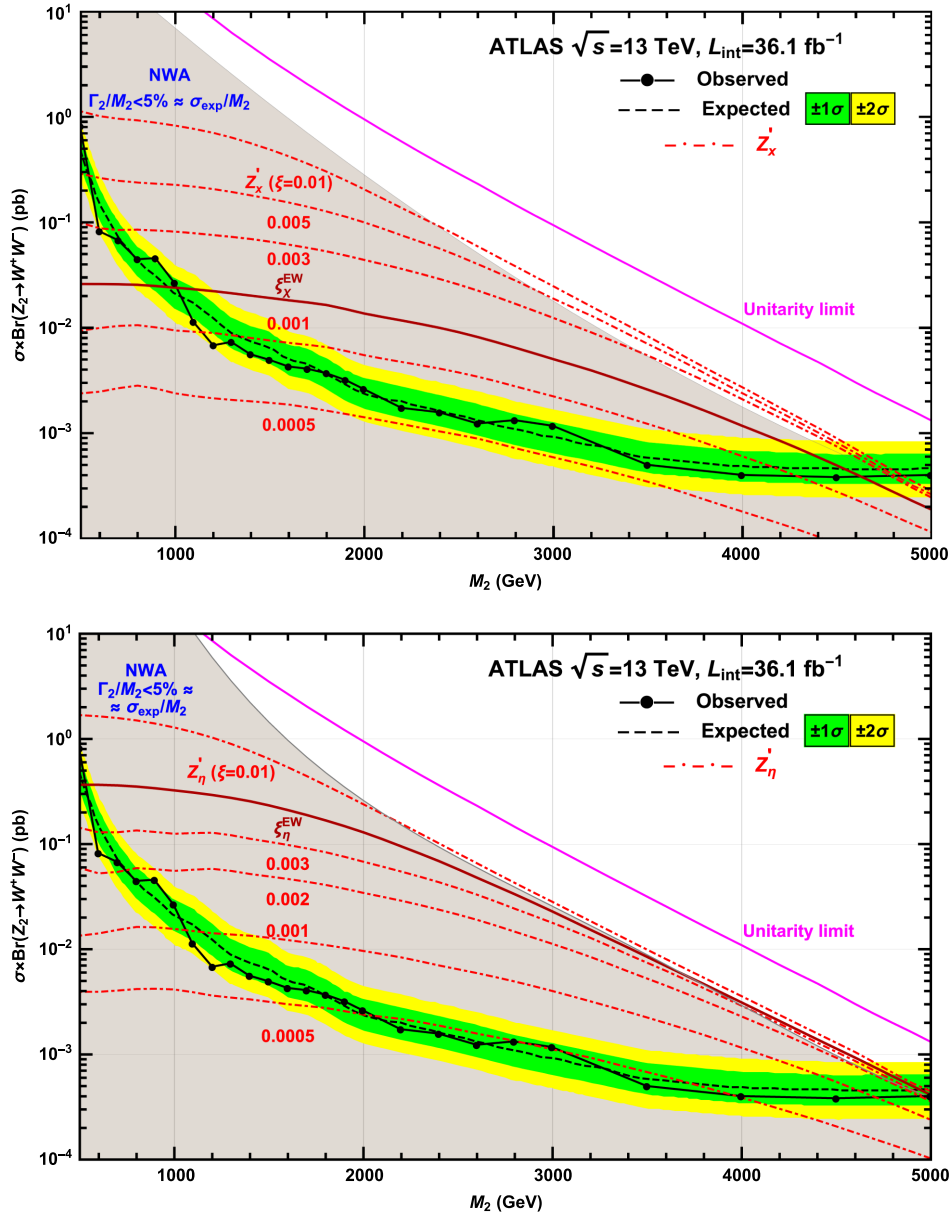
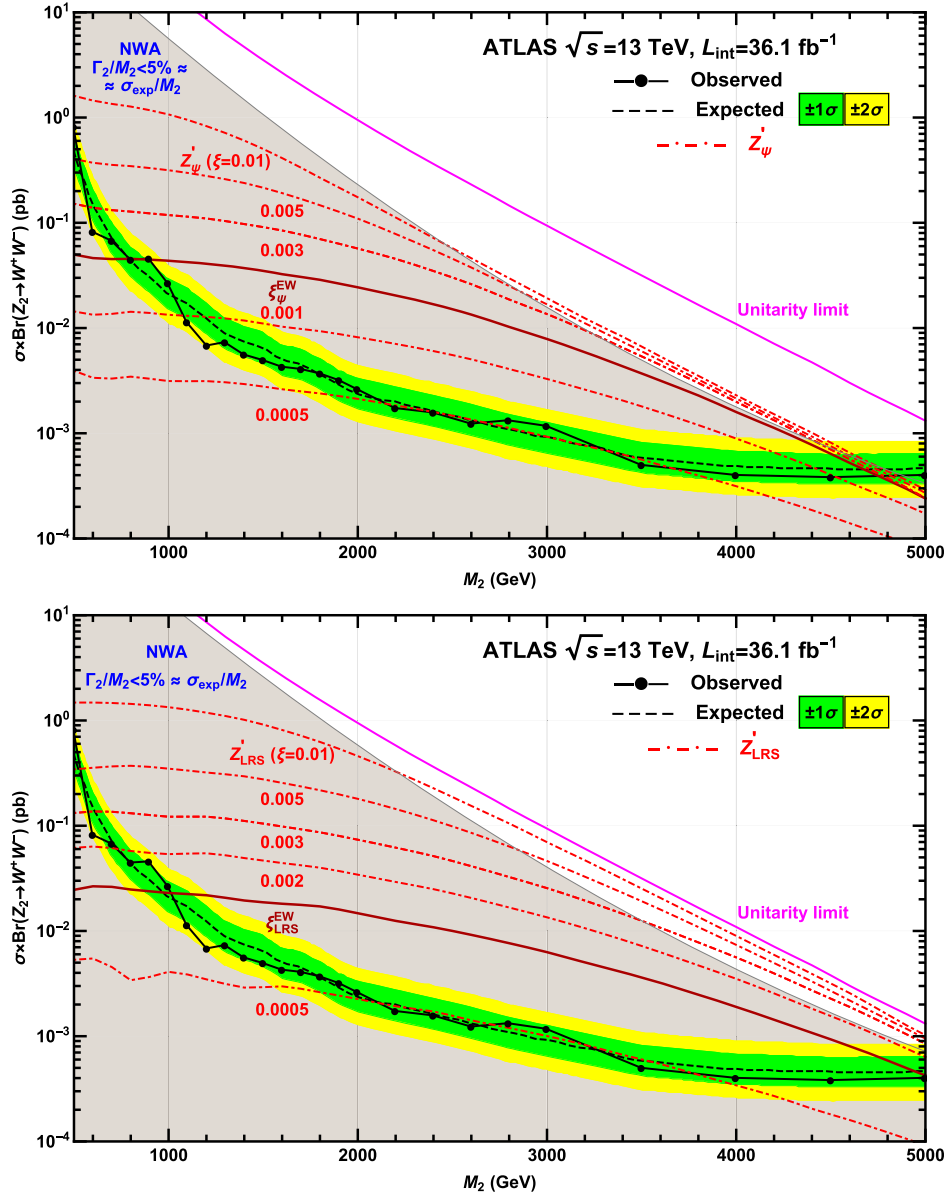


FIG. 5. Observed and expected 95% C.L. upper limits on the production cross section times the branching fraction for $Z_2 \rightarrow W^+W^-$ as a function of the Z_2 mass, M_2 , taken from Fig. 7(a) of Ref. [15], showing ATLAS data for 36.1 fb^{-1} . Theoretical production cross sections $\sigma \times \text{Br}(Z_2 \rightarrow W^+W^-)$ for the χ and η models (upper and lower panels, respectively) are calculated from PYTHIA 8.2 with a K -factor of 1.9, and given by dash-dotted curves, for mixing factor ξ ranging from 0.01 and down to 0.0005. Also, the cross section indicated by the solid line corresponds to the mixing parameter $\xi_{\text{model}}^{\text{EW}}$. The area indicated by gray corresponds to the region where the Z_2 resonance width is predicted to be less than 5% of the resonance mass, in which the narrow-resonance assumption is satisfied. The lower boundary of the region excluded by the unitarity violation arguments is also indicated.

[15]. We show in Figs. 5–7 the observed and expected 95% C.L. upper limits on the production cross section times the branching fraction, $\sigma \times \text{Br}(Z_2 \rightarrow W^+W^-)_{95\%}$, as a function of the Z_2 mass, M_2 . The data analyzed comprises pp collisions at $\sqrt{s} = 13 \text{ TeV}$, recorded by the ATLAS (36.1 fb^{-1}) detector [15] at the LHC. As mentioned above,

ATLAS [15] analyzed the W^+W^- production in the process (1) through the semileptonic final states.

Then, for Z_2 we compute the LHC production cross section multiplied by the branching ratio into two W bosons, $\sigma \times \text{Br}(Z_2 \rightarrow W^+W^-)_{\text{theory}}$, as a function of the two parameters (M_2, ξ), and compare it with the limits established by the


 FIG. 6. Same as in Fig. 5 but for the ψ model (upper) and the LRS model (lower panel).

ATLAS experiment, $\sigma \times \text{Br}(Z_2 \rightarrow W^+ W^-)_{95\%}$. Our strategy in the present analysis is to adopt the SM backgrounds that have been carefully evaluated by the experimental collaborations and simulate only the Z_2 signal.

In these figures, the inner (green) and outer (yellow) bands around the expected limits represent $\pm 1\sigma$ and $\pm 2\sigma$ uncertainties, respectively. The theoretical production cross sections $\sigma \times \text{Br}(Z_2 \rightarrow W^+ W^-)_{\text{theory}}$ for Z_2 bosons of the benchmark models are calculated from PYTHIA 8.2 [44], adapted for such kinds of analysis. Higher-order QCD corrections to the signal were estimated using a K -factor, for which we adopt a mass-independent value of 1.9

[45–47]. These theoretical curves for the cross sections, in descending order, correspond to values of the Z - Z' mixing factor ξ from 0.01 to 0.0005. The intersection points of the expected (and measured) upper limits on the production cross section with these theoretical cross sections for various ξ give the corresponding lower bounds on (M_2, ξ) , to be summarized in Sec. VII.

The signature space depicted in Figs. 5–7 is limited by the assumption that the resonance sought is narrow. The shaded area represents the region where the theoretical width Γ_2 is smaller than the experimental resolution ΔM ($\equiv \sigma_{\text{exp}}$) of the searches, and thus where the narrow-resonance assumption is

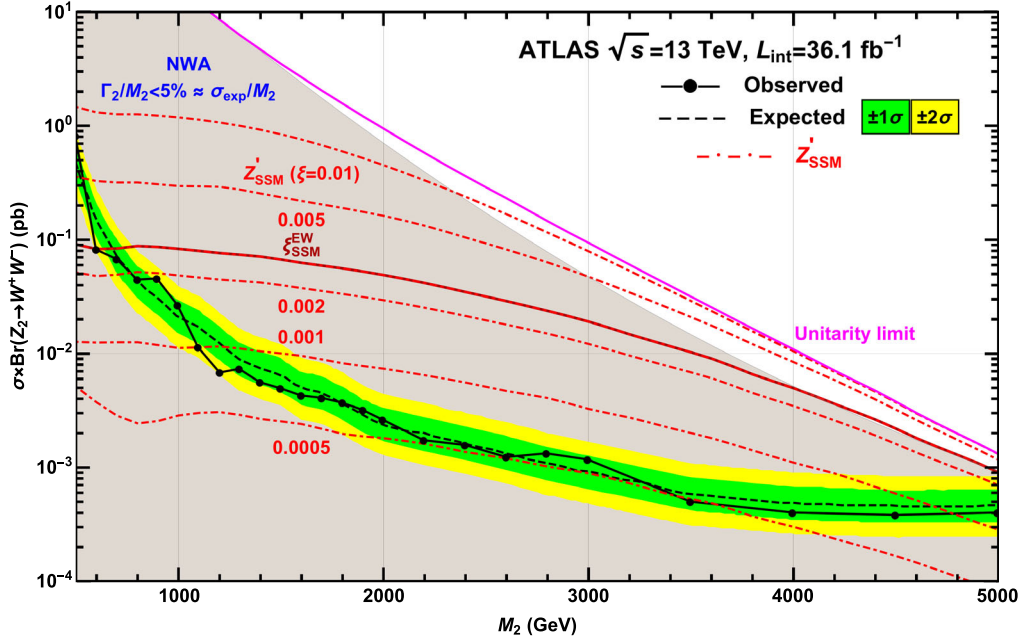


FIG. 7. Same as in Fig. 5 but for the SSM model.

satisfied. This region is defined by a predicted resonance width, relative to its mass, of at most 5%, corresponding to the best detector resolution of the searches.

In addition, in Figs. 5–7 we plot curves labeled “Unitarity limit” that correspond to the unitarity bound (see, e.g., [48] and references therein, where it was shown that the saturation of unitarity in the elastic scattering $W^+W^- \rightarrow W^+W^-$ leads to the constraint $g_{Z'WW_{\text{max}}} = g_{ZWW} \cdot (M_Z/\sqrt{3}M_{Z'})$). This constraint was adopted in plotting the unitarity bound. It was obtained under the assumption that the couplings of the Z' to quarks and to gauge bosons have the same Lorentz structure as those of the SM, but with rescaled strength.

The signature space displayed in Figs. 5–7 bounded by the curve labeled ξ^{EW} and the curve corresponding to the 95% C.L. upper limits, $\sigma \times \text{Br}(Z_2 \rightarrow W^+W^-)_{95\%}$, is excluded by the ATLAS experiment. It is interesting to note that for some range of mixing parameters ξ the Z_2 mass may be excluded up to approximately 5 TeV at 95% C.L., which slightly exceeds the sensitivity of the DY process.

VI. CONSTRAINTS FROM THE DRELL–YAN PROCESS

The above analysis was for the diboson process (1), employing the most recent ATLAS measurements [15]. Next, we turn to the Drell–Yan process; this process gives valuable complementary information. We compute the Z_2 production cross section at the LHC, σ , multiplied by the branching ratio into two leptons, l^+l^- ($l = e, \mu$), i.e., $\sigma \times \text{Br}(Z_2 \rightarrow l^+l^-)_{\text{theory}}$, as a function of M_2 , and compare it with the upper limits established by the experiment [3] for

36.1 fb^{-1} . Results for $\sigma \times \text{Br}(Z_2 \rightarrow l^+l^-)_{95\%}$ are shown in Fig. 8. To account for next-to-next-to-leading order (NNLO) effects in the QCD strong coupling constant, the leading order (LO) cross sections calculated with PYTHIA 8.2 [44] are multiplied by a mass-independent K -factor. The value of the K -factor is estimated at a dilepton invariant mass of 3.0–4.5 TeV and found to be consistent with unity [3,4].

For illustrative purposes we show theoretical production cross sections $\sigma \times \text{Br}(Z_2 \rightarrow l^+l^-)_{\text{theory}}$ for the Z_2 boson for only one representative model, ψ , given by the dash-dotted curves in Fig. 8. These curves, in descending order correspond to values of the mixing factor ξ from 0.0 to 0.01. Qualitatively, the decrease of the theoretical cross section with increasing values of ξ can be understood as follows: For increasing ξ , the $Z_2 \rightarrow W^+W^-$ mode will at high mass M_2 become more dominant (as illustrated in Figs. 2–4), and $\text{Br}(Z_2 \rightarrow l^+l^-)$ will decrease correspondingly. Notice also, that applying a mass dependent K -factor (which for this process is less than 1.04), the ψ model mass limit of the Z_2 changes by only $\sim \mathcal{O}(50 \text{ GeV})$, justifying the use of the simpler mass-independent K -factor [3,4].

Comparison of $\sigma \times \text{Br}(Z_2 \rightarrow l^+l^-)_{\text{theory}}$ vs $\sigma \times \text{Br}(Z_2 \rightarrow l^+l^-)_{95\%}$ displayed in Fig. 8 allows us to read off an allowed mixing for a given mass value; higher masses are allowed for smaller mixing, for the reason stated above. This analysis, illustrated here for the ψ model, can also be performed for the other benchmark models under consideration. That comparison can be translated into constraints on the two-dimensional $M_2 - \xi$ parameter plane, as will be shown in the next section.

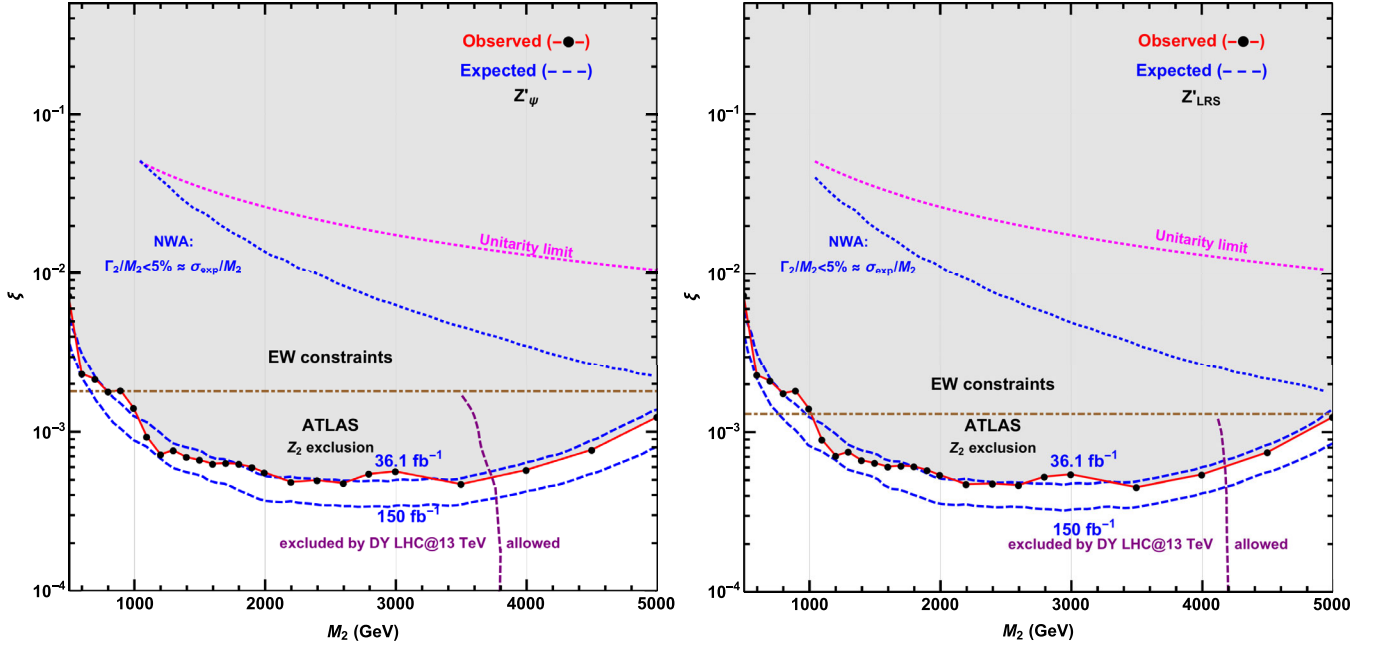


FIG. 10. Same as in Fig. 9 but for the ψ model (left panel) and the LRS model (right panel).

basically exclude masses $M_2 \lesssim 4$ TeV, with only a weak dependence on ξ . Also, we show the unitarity limits discussed above, as well as the upper bound for the validity of the NWA, both as dashed lines.

Interestingly, these figures show that at high Z_2 masses, the limits on ξ obtained from the ATLAS diboson resonance production search at 13 TeV are substantially stronger than those derived from the global analysis of the precision electroweak data [5], which are also displayed. In Fig. 11, which is dedicated to the SSM model,

we display limits on the Z_2 parameters from the Tevatron exclusion [7], the latter also based on the assumption that no decay channels into exotic fermions or superpartners are open.

Furthermore, we have extrapolated the experimental sensitivity curves for higher expected luminosity downwards by a factor of $1/\sqrt{D}$, where D is the ratio of the expected integrated luminosity of 150 fb^{-1} that will presumably be collected by the end of Run II, to the already analyzed integrated luminosity of 36.1 fb^{-1} in the ATLAS experiment. It is clear that further improvement on the constraining of this mixing can be achieved from the analysis of such data. It is easy to see that the exclusion constraint on ξ at fixed M_2 scales as $\sim \mathcal{L}_{\text{int}}^{-1/4}$ when statistical errors dominate. This scaling law $\sim \mathcal{L}_{\text{int}}^{-1/4}$ for the exclusion bound is an excellent approximation to what is demonstrated in Figs. 9–11 and in Table II.

In Table II, we collect our limits on the Z_2 parameters for the benchmark models. Also shown in Table II are the current limits on the Z - Z' mixing parameter ξ from LEP2 and Tevatron, derived from studies of diboson W^+W^- pair production. The limits on ξ at the Tevatron assume (as does the present study) that no decay channels into exotic fermions or superpartners are open to the Z_2 . Otherwise, the limits would be moderately weaker. LEP2 constrains virtual and Z - Z' boson mixing effects by the angular distribution of W bosons. Table II shows that the limits on ξ from the EW precision data are generally competitive with the future collider, ILC@0.5 TeV, and they are typically stronger than those from the preceding “low” energy colliders such as the Tevatron and LEP2. The LHC limits obtained at current c.m.s. pp energy, 13 TeV, and

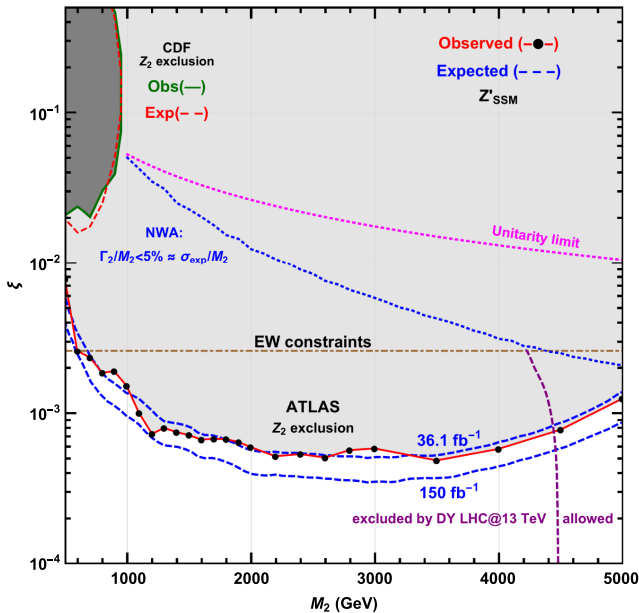


FIG. 11. Same as in Fig. 9 but for the SSM model.

time-integrated luminosity, $\mathcal{L}_{\text{int}} = 36.1 \text{ fb}^{-1}$, will improve the EW limits by a factor of order 3–10.

VIII. CONCLUDING REMARKS

The diboson production at LHC@13 TeV allows for the placement of stringent constraints on the Z - Z' mixing angle and Z_2 mass, M_2 . We derived limits on the mass and the Z - Z' mixing angle of the neutral Z_2 bosons by using data from pp collisions at $\sqrt{s} = 13 \text{ TeV}$ and recorded by the ATLAS detector at the CERN LHC, with integrated luminosity of $\sim 36 \text{ fb}^{-1}$. By comparing the experimental limits to the theoretical predictions for the total cross section of Z_2 resonant production and its subsequent decay into W^+W^- pairs, we show that the derived constraints on the Z - Z' mixing angle for the benchmark models are of the order of a few $\times 10^{-4}$, greatly improved with respect to those derived from the global analysis of electroweak data. Further improvement on the constraining of this mixing can be achieved from the analysis of data to be collected at higher luminosity expected in Run II. We also show that only the future e^+e^- linear collider ILC with polarized beams and with very high energy and luminosity, $\sqrt{s} = 1 \text{ TeV}$ and $\mathcal{L}_{\text{int}} = 1 \text{ ab}^{-1}$, may have a chance to compete with the LHC operating with presently used energy and luminosity.

Now, let us return to the issue concerning the second scenario considered in Sec. III. That scenario assumes that the partial widths are related, $\Gamma_2^{Z_1H} = \Gamma_2^{WW}$ for heavy M_2 .

Then Γ_2 would be larger by some factor, with a corresponding suppression in the branching ratio to W^+W^- , and the bounds from the LHC would be weaker. However, our calculations show that accounting for the contribution of the Z_2 boson decay channel, $Z_2 \rightarrow Z_1H$, to the total width Γ_2 does not dramatically change the bounds on the mixing parameter ξ obtained in the first scenario where $\Gamma_2^{Z_1H} = 0$. Namely, it turns out that the constraints on Z - Z' mixing are relaxed by at most 20–25% for the higher Z_2 masses.

In this paper, for the sake of compactness of the graphic material, we limited ourselves to an analysis of experimental data from the ATLAS detector only. Our further analysis shows that the corresponding CMS data [16] yields bounds on the mixing parameter ξ and the Z_2 boson mass that agree with the results based on ATLAS data. In addition, our recent comparative analysis presented in Ref. [13], based on the preliminary experimental data of the CMS detector at integrated luminosity of 35.9 fb^{-1} at 13 TeV, agrees with that performed with ATLAS data, confirming the equal sensitivity of the W -pair production process to Z' parameters within the SSM model.

ACKNOWLEDGMENTS

This research has been partially supported by the Abdus Salam International Centre for Theoretical Physics, OEA2973 and the Belarusian Republican Foundation for Fundamental Research, F17D-005. The work of P. O. has been supported by the Norges Forskningsråd.

-
- [1] P. Langacker, *Rev. Mod. Phys.* **81**, 1199 (2009).
 - [2] M. Tanabashi *et al.* (Particle Data Group), *Phys. Rev. D* **98**, 030001 (2018).
 - [3] M. Aaboud *et al.* (ATLAS Collaboration), *J. High Energy Phys.* **10** (2017) 182.
 - [4] A. M. Sirunyan *et al.* (CMS Collaboration), [arXiv:1803.06292](https://arxiv.org/abs/1803.06292).
 - [5] J. Erler, P. Langacker, S. Munir, and E. Rojas, *J. High Energy Phys.* **08** (2009) 017.
 - [6] F. del Aguila, J. de Blas, and M. Perez-Victoria, *J. High Energy Phys.* **09** (2010) 033.
 - [7] T. Aaltonen *et al.* (CDF Collaboration), *Phys. Rev. Lett.* **104**, 241801 (2010).
 - [8] V. V. Andreev and A. A. Pankov, *Yad. Fiz.* **75**, 67 (2012) [*Phys. At. Nucl.* **75**, 76 (2012)].
 - [9] S. Schael *et al.* (ALEPH, DELPHI, L3, OPAL, and SLD Collaborations and LEP Electroweak Working Group, SLD Electroweak Group, and SLD Heavy Flavour Group), *Phys. Rep.* **427**, 257 (2006).
 - [10] A. A. Pankov and C. Verzegnassi, *Phys. Lett. B* **233**, 259 (1989).
 - [11] P. Osland and A. A. Pankov, *Phys. Lett. B* **403**, 93 (1997).
 - [12] V. V. Andreev, P. Osland, and A. A. Pankov, *Phys. Rev. D* **90**, 055025 (2014).
 - [13] P. Osland, A. A. Pankov, and A. V. Tsytrinov, *Phys. Rev. D* **96**, 055040 (2017).
 - [14] G. Altarelli, B. Mele, and M. Ruiz-Altaba, *Z. Phys. C* **45**, 109 (1989); **47**, 676(E) (1990).
 - [15] M. Aaboud *et al.* (ATLAS Collaboration), *J. High Energy Phys.* **03** (2018) 042.
 - [16] A. M. Sirunyan *et al.* (CMS Collaboration), *Phys. Rev. D* **97**, 072006 (2018).
 - [17] D. Benchekrroun, C. Driouichi, and A. Hoummada, *Eur. Phys. J. Direct* **3**, N3 (2001).
 - [18] Internet <https://hepdata.net/>.
 - [19] A. A. Pankov and N. Paver, *Phys. Rev. D* **48**, 63 (1993).
 - [20] V. V. Andreev, G. Moortgat-Pick, P. Osland, A. A. Pankov, and N. Paver, *Eur. Phys. J. C* **72**, 2147 (2012).
 - [21] V. V. Andreev, A. A. Pankov, and V. A. Bednyakov, *Yad. Fiz.* **78**, 775 (2015) [*Phys. At. Nucl.* **78**, 725 (2015)].
 - [22] V. M. Abazov *et al.* (D0 Collaboration), *Phys. Rev. Lett.* **107**, 011801 (2011).
 - [23] G. Aad *et al.* (ATLAS Collaboration), *Phys. Lett. B* **718**, 860 (2013).

- [24] G. Aad *et al.* (ATLAS Collaboration), *Phys. Lett. B* **712**, 331 (2012).
- [25] G. Aad *et al.* (ATLAS Collaboration), *Phys. Lett. B* **737**, 223 (2014).
- [26] V. Khachatryan *et al.* (CMS Collaboration), *Phys. Lett. B* **740**, 83 (2015).
- [27] M. Aaboud *et al.* (ATLAS Collaboration), *J. High Energy Phys.* **09** (2016) 173.
- [28] V. Khachatryan *et al.* (CMS Collaboration), *J. High Energy Phys.* **08** (2014) 174.
- [29] A. M. Sirunyan *et al.* (CMS Collaboration), *J. High Energy Phys.* **03** (2017) 162.
- [30] T. G. Rizzo, [arXiv:hep-ph/0610104](https://arxiv.org/abs/hep-ph/0610104).
- [31] P. Langacker and M. x. Luo, *Phys. Rev. D* **45**, 278 (1992).
- [32] B. Holdom, *Phys. Lett.* **166B**, 196 (1986).
- [33] M. E. Krauss, B. O’Leary, W. Porod, and F. Staub, *Phys. Rev. D* **86**, 055017 (2012).
- [34] M. Hirsch, W. Porod, L. Reichert, and F. Staub, *Phys. Rev. D* **86**, 093018 (2012).
- [35] J. Pumplin, D. R. Stump, J. Huston, H. L. Lai, P. M. Nadolsky, and W. K. Tung, *J. High Energy Phys.* **07** (2002) 012.
- [36] G. Aad *et al.* (ATLAS Collaboration), *Phys. Rev. D* **87**, 112001 (2013); **88**, 079906(E) (2013).
- [37] V. Barger, P. Langacker, and H. S. Lee, *Phys. Rev. Lett.* **103**, 251802 (2009).
- [38] J. Kang and P. Langacker, *Phys. Rev. D* **71**, 035014 (2005).
- [39] E. Salvioni, G. Villadoro, and F. Zwirner, *J. High Energy Phys.* **11** (2009) 068.
- [40] M. S. Chanowitz and M. K. Gaillard, *Nucl. Phys.* **B261**, 379 (1985).
- [41] V. D. Barger and K. Whisnant, *Phys. Rev. D* **36**, 3429 (1987).
- [42] C. Dib and F. J. Gilman, *Phys. Rev. D* **36**, 1337 (1987).
- [43] A. M. Sirunyan *et al.* (CMS Collaboration), *Phys. Lett. B* **774**, 533 (2017).
- [44] T. Sjostrand, S. Ask, J. R. Christiansen, R. Corke, N. Desai, P. Ilten, S. Mrenna, S. Prestel, Christine O. Rasmussen, and P. Z. Skands, *Comput. Phys. Commun.* **191**, 159 (2015).
- [45] S. Frixione, *Nucl. Phys.* **B410**, 280 (1993).
- [46] N. Agarwal, V. Ravindran, V. K. Tiwari, and A. Tripathi, *Phys. Lett. B* **690**, 390 (2010).
- [47] T. Gehrmann, M. Grazzini, S. Kallweit, P. Maierhöfer, A. von Manteuffel, S. Pozzorini, D. Rathlev, and L. Tancredi, *Phys. Rev. Lett.* **113**, 212001 (2014).
- [48] A. Alves, O. J. P. Eboli, D. Goncalves, M. C. Gonzalez-Garcia, and J. K. Mizukoshi, *Phys. Rev. D* **80**, 073011 (2009).